Experimental Investigation of Multistage Interaction Gust Aerodynamics

V. R. Capece[1]

S. Fleeter

Thermal Sciences and Propulsion Center,
School of Mechanical Engineering,
Purdue University,
West Lafayette, IN 47907

The fundamental flow physics of multistage blade row interactions are experimentally investigated at realistic reduced frequency values. Unique data are obtained that describe the fundamental unsteady aerodynamic interaction phenomena on the stator vanes of a three-stage axial flow research compressor. In these experiments, the effect on vane row unsteady aerodynamics of the following are investigated and quantified: (1) steady vane aerodynamic loading; (2) aerodynamic forcing function waveform, including both the chordwise and transverse gust components; (3) solidity; (4) potential interactions; and (5) isolated airfoil steady flow separation.

Introduction

Airfoil rows of advanced gas turbine engines are susceptible to destructive aerodynamically induced vibrational responses, with upstream blade and vane wakes the most common excitation source. For example, in the single-stage compressor flow field schematically depicted in Fig. 1, the rotor wake velocity deficits appear as a temporally varying excitation source to a coordinate system fixed to the downstream stator vanes, i.e., the rotor blade wakes are the forcing function to the downstream stator vanes. Also as shown, the reduction of the rotor relative velocity causes a decrease in the absolute velocity and increases the incidence to the stator vanes. This produces a fluctuating aerodynamic lift and moment on the vanes, which can result in high vibratory stress and high cycle fatigue failure.

First-principle forced response predictive techniques require a definition of the unsteady forcing function in terms of harmonics. The total response of the airfoil to each harmonic is then assumed to be comprised of two parts. One is due to the disturbance being swept past nonresponding airfoils. The second arises when the airfoils respond to the forcing function. A gust analysis predicts the unsteady aerodynamics of the nonresponding airfoils, with a harmonically oscillating airfoil analysis used to predict the additional motion-induced unsteady aerodynamics.

Both gust and harmonically oscillating unsteady aerodynamic models are being developed (e.g., Fleeter, 1973; Verdon and Caspar, 1981; Englert, 1982; Atassi, 1984; Chiang and Fleeter, 1988). Within these models are many numerical, analytical, and physical assumptions. Unfortunately, there is only a limited quantity of high reduced frequency data appropriate for model verification and direction.

Carta and St. Hilaire (1979) and Carta (1982) measured the surface chordwise unsteady pressure distribution on an harmonically oscillating cascade in a linear wind tunnel. This work was extended by Hardin et al. (1987) to an isolated rotor with oscillating blades. In addition, inlet distortion generated gust response unsteady aerodynamics were also studied. Although the interblade phase angles in these experiments were within the range found in turbomachines, the reduced frequencies, less than 0.4, were low for forced response unsteady aerodyanmics found in the mid and aft stages of multistage turbomachines where the reduced frequency is typically greater than 2.0. Fleeter et al. (1978, 1980, 1981) investigated the effects of airfoil profile and rotor–stator axial

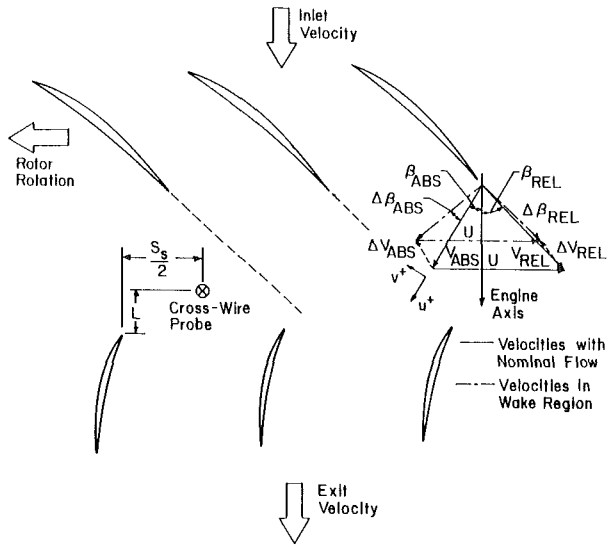

Fig. 1 Single-stage compressor flow field

[1]Currently at Pratt & Whitney Engineering Division South.

Contributed by the International Gas Turbine Institute and presented at the 33rd International Gas Turbine and Aeroengine Congress and Exhibition, Amsterdam, The Netherlands, June 5–9, 1988. Manuscript received at ASME Headquarters February 11, 1988. Paper No. 88-GT-56.

Table 1 Overall compressor and airfoil characteristics

	ROTOR	STATOR
Airfoil Type	C4	C4
Number of Airfoils	43	41
Chord, C (mm)	30	30
Solidity, C/S	1.14	1.09
Camber, θ	27.95	27.70
Stagger Angle, λ	36	-36.1
Aspect Ratio	2.0	2.0
Thickness/Chord (%)	10	10
Axial Gap (cm)	1.27	
Flow Rate (kg/s)	2.66	
Design Axial Velocity (m/s)	32.0	
Rotational Speed (RPM)	3000	
Number of Stages	3	
Stage Pressure Ratio	1.003	
Inlet Tip Diameter (mm)	420	
Hub/Tip Radius Ratio	0.714	
Stage Efficiency (%)	85	

spacing on the transverse gust unsteady aerodynamic response in a single-stage, low-speed research compressor at realistic values of the reduced frequency, with these data also showing the influence of the forcing function waveform.

These previous experimental investigations were performed in linear cascades, isolated rotor rows, and single-stage compressors. They did not consider the multistage and potential interaction effects that exist in the mid and aft stages of turbomachines. For multistage compressors, the unsteady aerodynamics on the first two vane rows of a three-stage low-speed research compressor were studied for the first time by Capece et al. (1986). The transverse gust forcing function and the chordwise distributions of the harmonic pressure difference coefficients on the first two vane rows were determined for a variety of geometric and compressor operating conditions. These results indicated that the unsteady aerodynamic loading of an airfoil row was related to the aerodynamic forcing function, which itself is significantly influenced by the multistage blade row interactions. This work was extended by Capece and Fleeter (1987) to include all three vane rows, with the effects of both the transverse and chordwise gust components quantified.

In this paper, the fundamental flow physics of multistage blade row interactions are experimentally investigated at realistic reduced frequency values, with unique data obtained to describe the fundamental unsteady aerodynamic phenomena on the stator vanes of a three-stage research compressor. In particular, a series of experiments are performed to investigate and quantify the effect of the following on vane row unsteady aerodynamics: (1) steady loading; (2) forcing function waveform, including both the chordwise and transverse gust components; (3) solidity; (4) potential interactions, and (5) steady flow separation.

Research Compressor and Instrumentation

The Purdue University Three-Stage Axial Flow Research Compressor is driven by a 15 hp d-c electric motor over a speed range of 300 to 3000 rpm. The three identical compressor stages consist of 43 rotor blades and 41 stator vanes, with the first-stage rotor inlet flow field controlled by variable setting angle inlet guide vanes. The free-vortex design airfoils have a British C4 section profile, a chord of 30 mm, an aspect ratio of 2, and a maximum thickness-to-chord ratio of 0.10. The overall airfoil and compressor characteristics are presented in Table 1.

The aerodynamic forcing functions to the stator rows are the upstream airfoil wakes. The first-stage vane row forcing function is varied by changing the setting angle of the inlet guide vanes, thereby altering the inlet flow to the first stage rotor (Fig. 2). This results in a change in the rotor blade exit flow field, in particular, the chordwise and transverse gust components. The second and third-stage vane row forcing function variations are accomplished by independently circumferentially indexing the upstream vane rows relative to one another, as also depicted.

The stator vane forcing function is quantified by measuring the stator inlet time-variant velocity and flow angle with a cross-wire probe located midway between rotor and stator at midstator circumferential spacing (Fig. 1). The rotor mean absolute exit flow angle is determined by rotating the probe until a zero voltage difference is obtained between the two hot-wire channels. This mean angle is then used as a reference for calculating the instantaneous absolute and relative flow angles and defines the vane steady incidence angle. From the instantaneous velocity triangles, the individual fluctuating velocity components parallel and normal to the mean flow, the aerodynamic gust components, are calculated. The accuracy of the velocity magnitude and angle are ± 4 percent and ± 2 deg, respectively.

The steady and unsteady aerodynamic loading on the vane surfaces are measured with chordwise distributions of midspan surface pressure taps and tranducers. Flow visualization along this streamline shows the flow to be two dimensional for the operating conditions of this investigation. A

Nomenclature

C = vane chord
$\bar{C}_l$ = steady lift coefficient $= \int_0^C (\bar{p}_p - \bar{p}_s)dx \Big/ \frac{1}{2}\rho U_t^2 C$
C_p = first harmonic dynamic pressure coefficient $= \Delta\hat{p}/\rho V_x \hat{v}^+$
$\bar{C}_p$ = static pressure coefficient $= (\bar{p} - \bar{p}_{exit}) \Big/ \frac{1}{2}\rho U_t^2$
i = incidence angle
k = reduced frequency $= \omega C/2V_x$
$\bar{p}$ = stator surface static pressure
$\bar{p}_{exit}$ = stator exit static pressure
$\Delta\hat{p}$ = first harmonic dynamic pressure difference
u^+ = instantaneous chordwise gust component
$\hat{u}^+$ = first harmonic chordwise gust
U_t = blade tip speed
v^+ = instantaneous transverse gust component
$\hat{v}^+$ = first harmonic transverse gust
V_x = absolute axial velocity
$\bar{\sigma}$ = solidity
ω = blade passing frequency

reverse transducer mounting technique is utilized to minimize disturbances, with the transducer connected to the measurement surface by a pressure tap. Static and dynamic calibrations of the embedded transducers demonstrate no hysteresis, with the mounting method not affecting the frequency response. The accuracy of the unsteady pressure measurements is ±3.5 percent.

Data Acquisition and Analysis

The steady-state data define the steady aerodynamic loading on the vane surfaces and the compressor operating point. A root-mean-square error analysis is performed, with the steady data defined as the mean of 30 samples and their 95 percent confidence intervals determined. The detailed steady loading on the vanes is defined by the chordwise distribution of the vane surface steady static pressure coefficient $\bar{C}_p$, with the overall loading level specified by the incidence angle i and the steady lift coefficient $\bar{C}_l$.

The time-variant data quantify the aerodynamic forcing function and the resulting unsteady pressure difference on the stator vanes, and are analyzed by means of a data-averaging or signal enhancement concept, as proposed by Gostelow (1977). The key to this technique is the sampling of data at a preset time, which is accomplished with a shaft-mounted optical encoder. At a steady-state operating point, an averaged time-variant data set consisting of the two hot-wire and the vane-mounted transducer signals, digitized at a rate of 200 kHz and averaged over 200 rotor revolutions, is obtained. Each is Fourier decomposed into harmonics by means of a Fast Fourier Transform algorithm, with the magnitude and phase angle of the first harmonic referenced to the data initiation pulse determined. Analyzing the data in this form was found to be equivalent to averaging the Fourier transforms for each rotor revolution. Also, ensemble averaging and then Fourier decomposing of the signal is used because it significantly reduces the data storage requirements.

The rotor and stator spacing, the axial spacing between the vane leading edge plane and the probe, and the absolute and relative flow angles are known. To time relate the hot wire and vane surface unsteady pressure signals, the rotor exit velocity triangles are examined and the following asumptions made: (1) The wakes are identical at the hot wire and stator leading edge planes, and (2) the wakes are fixed in the relative frame. The wakes are located relative to the hot wires and the leading edges of the instrumented vanes and the times at which the wakes are present at various locations determined. The incremented times between occurrences at the hot wire and the vane leading edge planes are then related to phase differences between unsteady velocities and the vane surfaces. These assumptions are necessary in order to correlate the data with a gust analysis, which fixes the gust at the airfoil leading edge. The hot wire was located approximately midway between the rotor and stator and was less than 25 percent of the stator chord upstream of its leading edge.

In final form, the detailed waveform of the aerodynamic forcing function is specified by the first harmonics of the chordwise and transverse gust components, $\hat{u}^+$ and $\hat{v}^+$, respectively. The unsteady pressure data describe the chordwise variation of the first harmonic pressure difference across a stator vane, presented as a dynamic pressure difference coefficient magnitude and phase. As a reference, these data are correlated with predictions from Fleeter (1973). This gust analysis assumes the flow to be inviscid, irrotational, two dimensional, and compressible. Small unsteady transverse velocity perturbations, v^+, are assumed to be convected with the uniform flow past a cascade of flat plate airfoils. The parameters modeled include the cascade solidity, stagger angle, inlet Mach number, reduced frequency, and the interblade phase angle. The analysis does not consider flow separation or chordwise gust perturbations u^+.

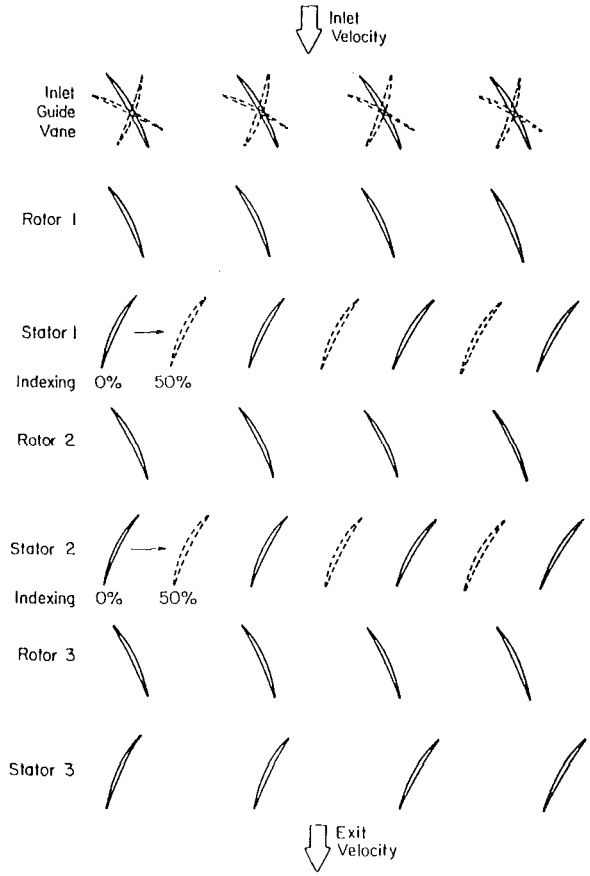

Fig. 2 Compressor geometry variations to alter forcing function

Results

Three stator vane solidities are investigated: the design value of 1.09; a reduced value of 0.545; and 0.10, which results in a spacing between vanes large enough so that the influence of neighboring vanes is negligible; i.e., each vane is an isolated airfoil. The results are presented for each solidity for variations in one of the key parameters. All design solidity data, except for the potential interaction effects, are presented for the first stator vane row. The data sets for the other solidities are presented for the third stator vane row. Since there are no airfoil rows downstream of the third stage vane row, there are no potential interaction effects on the trailing edge region of these vanes. Data from Capece and Fleeter (1987) have been added for the design solidity in order to have a complete presentation of the results and to indicate the significant effects that solidity has on the unsteady aerodynamic response of the stator vanes. Also, the error in the static pressure coefficient data is represented by the symbol size.

Vane Steady Loading

Steady aerodynamic loading effects are considered for the design and reduced solidities of 1.09 and 0.545. The first harmonics of the forcing function are maintained nearly constant (Fig. 3). Note that relative to the absolute velocity, the instantaneous gust components are not small. For example, the instantaneous transverse and chordwise gust components are approximately 40 and 25 percent of the absolute velocity at −5.9 deg of incidence. However, in terms of the first harmonics these gust components are approximately 11 and 6 percent of the absolute velocity.

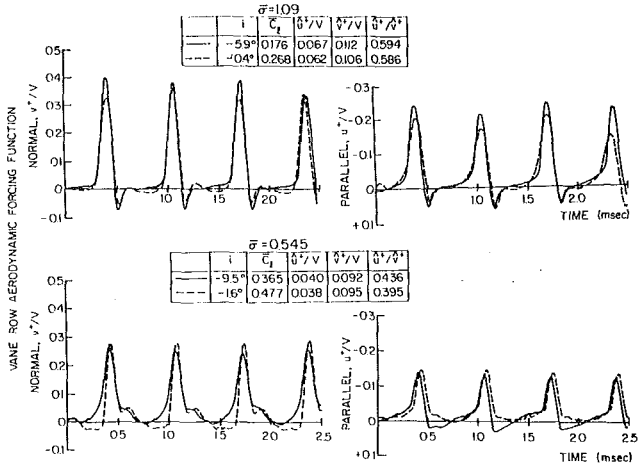

Fig. 3 Aerodynamic forcing functions for steady loading study

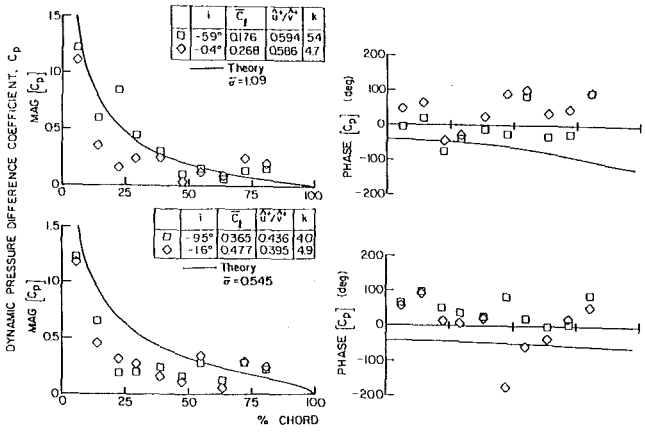

Fig. 5 Effect of steady loading on the complex unsteady pressure coefficient

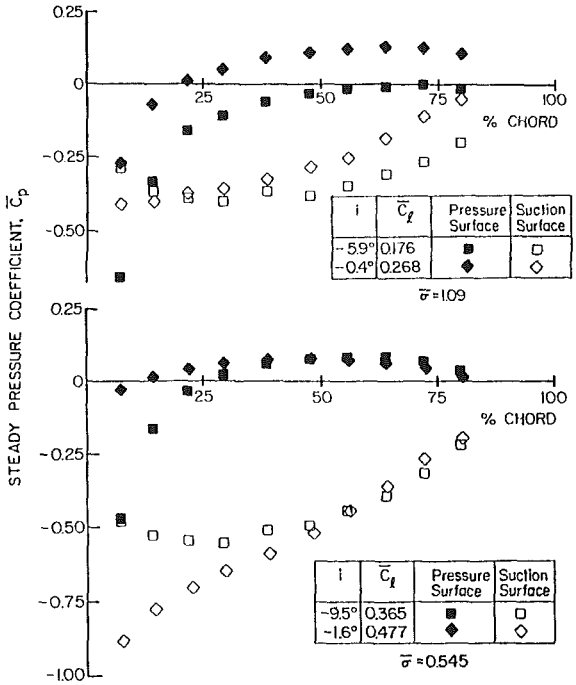

Fig. 4 Vane static pressure distributions for steady loading study

For each solidity, the vane surface steady pressure distributions are smooth and show no indication of flow separation (Fig. 4). At the design solidity, the surface static pressures for the lift coefficient of 0.268 are greater than those for the lift coefficient of 0.176, a result of the inlet guide vane indexing altering the compressor operating point. Also, the reduced solidity has much higher pressure differences and steady lift coefficients due to the decreased number of vanes.

The resulting chordwise distributions of the dynamic pressure difference coefficient and the predictions are shown in Fig. 5. At the design solidity, good correlation exists between the magnitude data and the prediction for the lift coefficient of 0.176, with an increase in lift to 0.268 resulting in poorer correlation. The higher loading data are decreased in amplitude relative to both the prediction and the lower loading data over the front 25 percent of the vane. Aft of 25 percent chord, the data correlate well with each other and the prediction until 63 percent chord, with both data sets then increasing to a larger value than the prediction.

The phase data exhibit a somewhat different chordwise distribution than the prediction. In particular, the phase data are increased relative to the prediction over the first 14 percent of vane chord. The data then decrease to the level of the prediction and then increase to values greater than the prediction with increasing chordwise position. The phase data for both loading levels exhibit the same trends, with the higher loading data increased relative to both the prediction and the lower loading data over most of the chord. The differences between the phase data and the prediction are attributed to the vane camber and the detailed steady loading distributions on the vane surfaces.

The magnitude data for the reduced solidity are also decreased relative to the prediction over the front 50 percent of the vane, with the higher loading data having, in general, a decreased amplitude relative to the lower loading data. The decrease in amplitude relative to the prediction is due to the high levels of steady aerodynamic loading. Aft of 50 percent chord, the magnitude data increase to the level of the prediction and show better correlation. The phase data increase to a level larger than the prediction over the front 14 percent of the vane, then decrease toward the prediction, and from approximately 25 to 50 percent chord, the phase data are almost constant. Aft of 50 percent chord this trend changes, with the higher loading data decreased relative to both the lower loading data and the prediction, and then increasing as the chordwise position increases. Thus, from these results it is evident that steady loading primarily affects the magnitude of the dynamic pressure difference coefficient.

The best correlation of the dynamic pressure difference coefficient data and the prediction is obtained at the low level of steady loading at the design solidity, as expected, since this most closely approximates the unloaded flat plate cascade model. Also, the steady loading level and distribution have a significant effect on the unsteady aerodynamics of the vane row. In general, different airfoil designs will produce different steady surface pressure distributions and steady lift for the same incidence angle. Therefore, the level of steady aerodynamic loading, not the incidence angle, is the key parameter in obtaining good correlation with mathematical models.

Aerodynamic Forcing Function

The influence of each gust component on the complex dynamic pressure coefficient, with the steady aerodynamic loading held constant, is considered.

Transverse Gust. The surface static pressure distributions for each solidity are smooth, with no evidence of separation and only small variations apparent near the leading edge, which result in the slight variations in the steady lift coeffi-

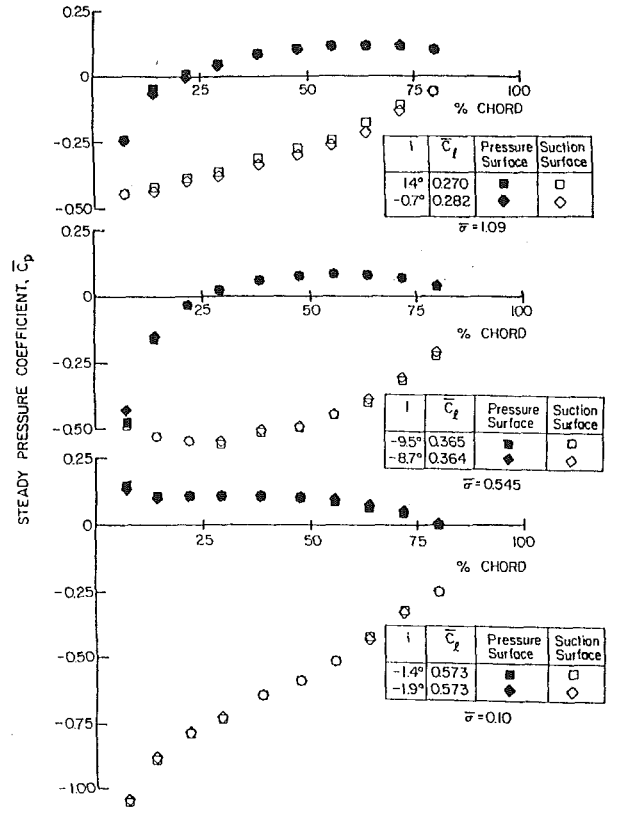

Fig. 6 Surface static pressure distributions for transverse gust study

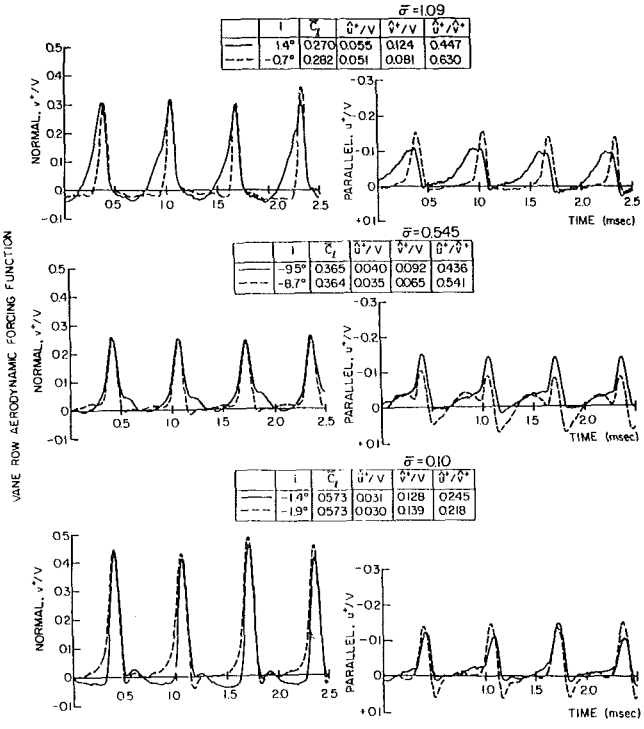

Fig. 7 Aerodynamic forcing functions for transverse gust study

cients (Fig. 6). As the solidity is decreased, there is an increase in the level of steady surface pressures and a corresponding increase in the steady lift coefficient. The chordwise gust $\hat{u}^+$ is held approximately constant while the transverse gust $\hat{v}^+$ is varied (Fig. 7), with the difference between the configurations specified by the first harmonic gust ratio $\hat{u}^+/\hat{v}^+$.

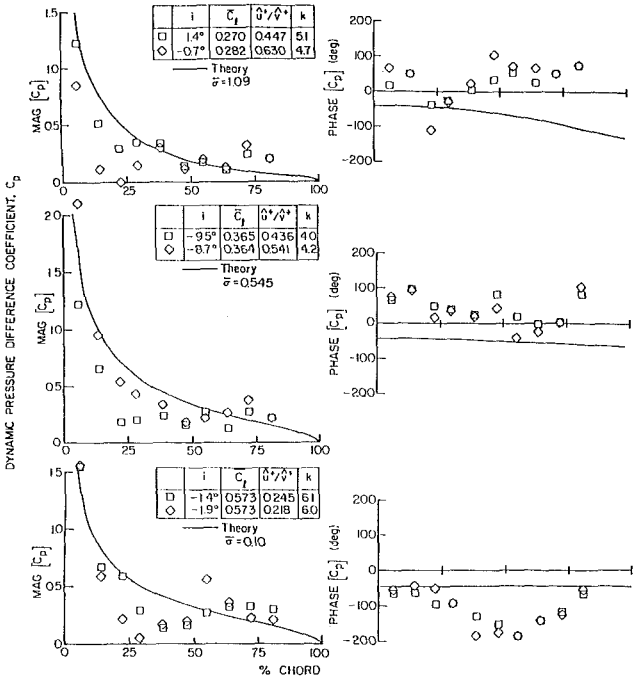

Fig. 8 Effect of transverse gust on the complex unsteady pressure coefficient

The effect of the transverse gust on the chordwise distributions of the dynamic pressure difference coefficient data is presented in Fig. 8. At the design solidity, both configurations show the magnitude data to be decreased relative to the prediction over the leading 30 percent of the vane, with the $(\hat{u}^+/\hat{v}^+)$ data of 0.630 having a decreased amplitude relative to the 0.447 data. However, in the midchord region, the data for these two configurations correlate well with each other and with the prediction. As in the previous cases, aft of 70 percent chord the data increase relative to the prediction. This is a result of both the potential interaction from the downstream second-stage rotor row and the parallel gust component $\hat{u}^+$, as the design solidity data are acquired on the first stage. This phenomenon will be discussed in greater detail in the section on Potential Flow Interactions.

The reduced solidity and the isolated airfoil data show a different trend with the ratio of $(\hat{u}^+/\hat{v}^+)$ than that of the design solidity, with the data for the larger values of $(\hat{u}^+/\hat{v}^+)$ increased in value relative to the lower values. This is opposite to the trend noted at the design solidity. However, examination of the magnitudes of the first harmonics of the chordwise gust component $\hat{u}^+$ indicates that the magnitudes of the chordwise gust are lower in value than the design case. This indicates that the chordwise pressure distributions are not governed simply by the ratio of the two gust components but also by their magnitudes.

For each of the reduced solidity values, 0.545 and 0.10, the magnitude data are generally decreased relative to the prediction over the leading 50 percent of the vane, with the lower $(\hat{u}^+/\hat{v}^+)$ data having a decreased amplitude relative to the higher $(\hat{u}^+/\hat{v}^+)$ data. In the trailing edge portion of the vane, the magnitude data correlate well with each other but are increased in level relative to the prediction. This is a result of the chordwise gust, which is not considered by the model.

The design solidity phase data are increased relative to the prediction over the front 14 percent of the vane, decrease to the level of the prediction at 22 percent chord, and then increase to values greater than the prediction with increasing chordwise position, becoming nearly constant aft of 40 percent chord. At the reduced solidity, the phase data are in-

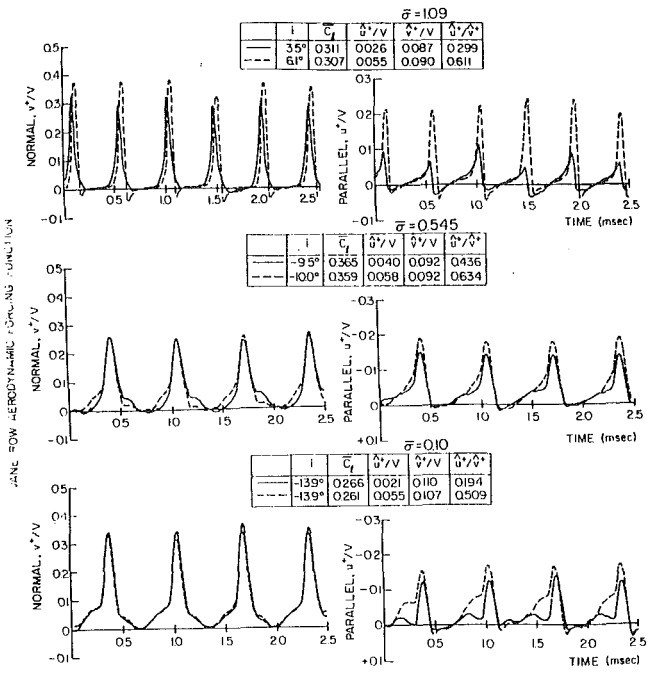

Fig. 9 Aerodynamic forcing function for chordwise gust study

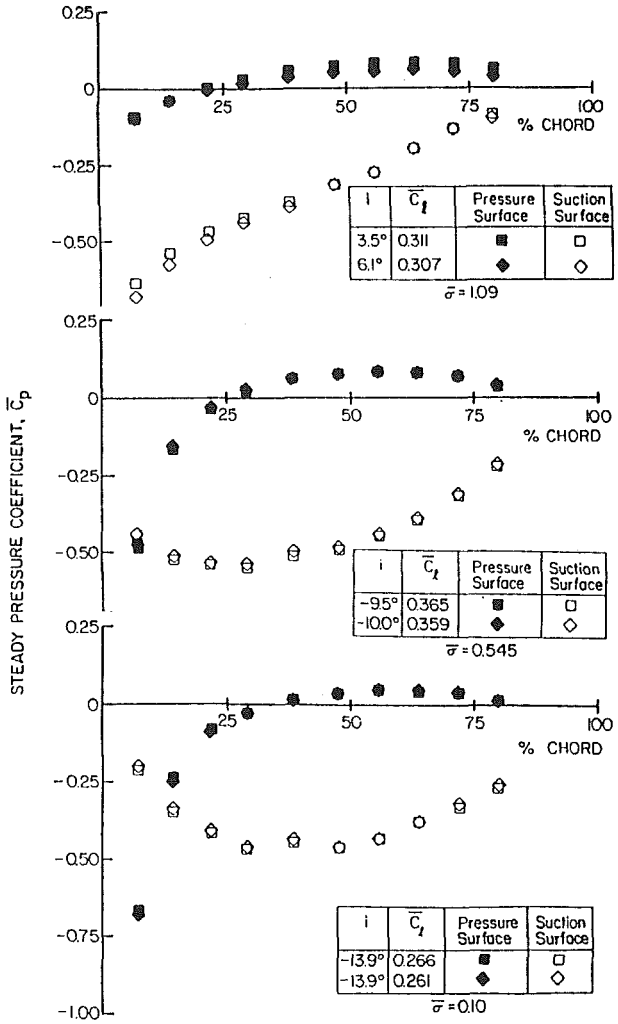

Fig. 10 Steady vane loading distributions for chordwise gust study

creased relative to the prediction over the entire vane chord, being nearly constant in the 22 to 38 percent chord region. For the isolated airfoil, the phase data show good trendwise correlation with the prediction over the leading 29 percent of the vane, with the $(\hat{u}^+/\hat{v}^+)$ data of 0.245 decreasing relative to both the prediction and the $(\hat{u}^+/\hat{v}^+)$ 0.218 data. Aft of 29 percent chord, where the vane does most of its turning, the phase data decrease until 54 percent chord and then increase with increasing chordwise position.

These results show that the transverse gust primarily influences the magnitude of the dynamic pressure difference coefficient. Also, the unsteady data variations with forcing function waveform cannot be predicted by harmonic gust models. This is because the forcing function waveforms and the resulting unsteady pressure distributions have been Fourier decomposed, with the first harmonic of the unsteady data presented. Thus, all of these first harmonic data are correlated with the same prediction curve; i.e., the predictions from these harmonic gust models are identical for all of the forcing function waveforms.

Chordwise Gust. The effect of the forcing function chordwise gust component $\hat{u}^+$ on the vane row unsteady aerodynamics for each solidity is considered. This is accomplished by establishing compressor configurations such that the transverse gust and the steady aerodynamic loading are nearly identical; see Figs. 9 and 10, respectively.

The resulting chordwise distributions of the dynamic pressure coefficient data and the predictions are presented in Fig. 11. In general, the magnitude data exhibit analogous trends for each solidity, decreasing over the front of the vane and increasing over the aft part. The magnitude data increase over the prediction at the design solidity, whereas they increase up to the prediction for the other two solidity values. This is again the result of the design solidity data being acquired on the first stage, with the data for the other solidities being acquired on the third stage. Also, the higher $(\hat{u}^+/\hat{v}^+)$ data are decreased relative to both the prediction and the lower $(\hat{u}^+/\hat{v})$ data for each solidity. This is particularly apparent at the design and reduced solidity.

The design solidity phase data at a $(\hat{u}^+/\hat{v}^+)$ of 0.611 show good trendwise correlation with the prediction over the aft 50

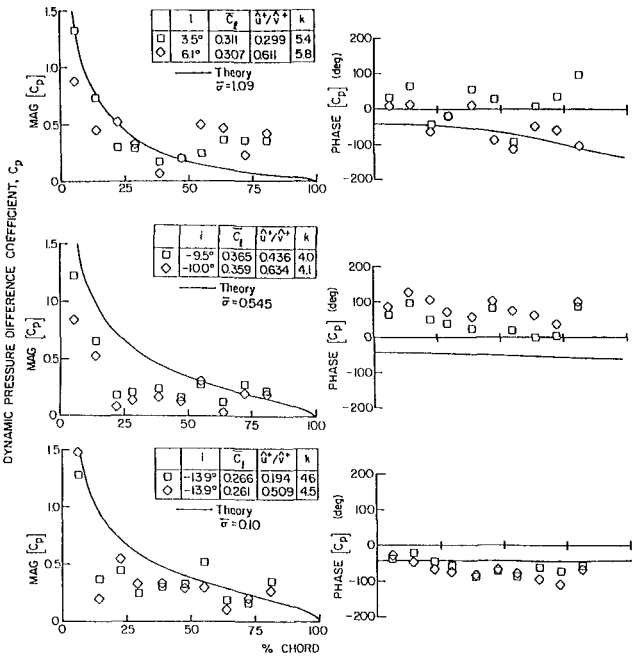

Fig. 11 Effect of chordwise gust on the complex unsteady pressure coefficient

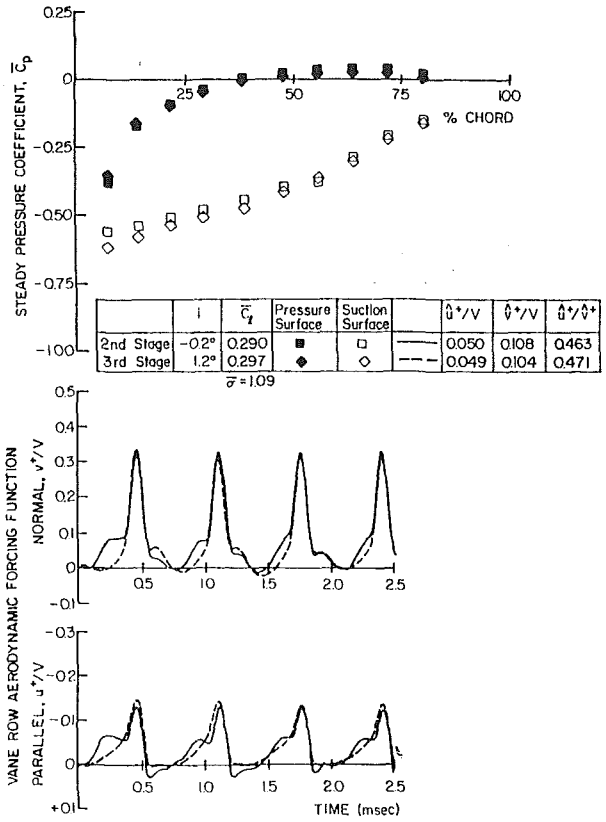

Fig. 12 Steady loading and forcing functions for potential flow interaction study

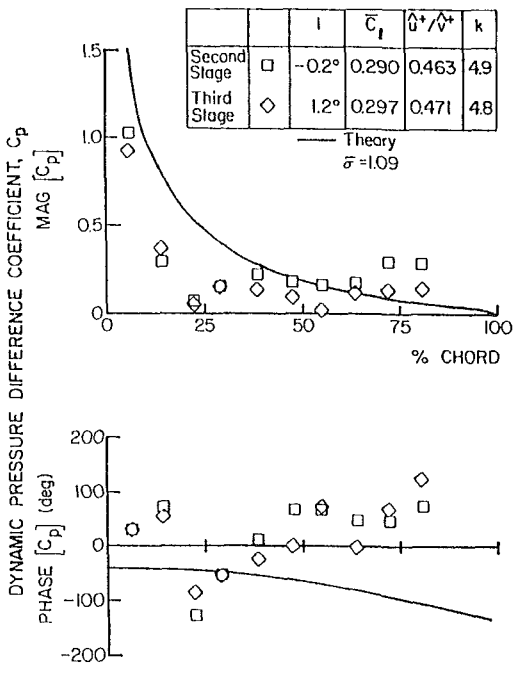

Fig. 13 Potential flow interaction effect on the complex unsteady pressure coefficient

percent of the vane while the lower $(\hat{u}^+/\hat{v}^+)$ data are increased relative to the prediction, as seen in previous cases. Over the front 50 percent of the vane, the data correlate trendwise with each other but are increased compared to the prediction. The reduced solidity phase data are increased relative to the prediction and remain relatively constant over the entire vane chord, with the $(\hat{u}^+/\hat{v}^+)$ phase data of 0.634 consistently increased over the $(\hat{u}^+/\hat{v}^+)$ 0.436 data.

A somewhat different trend is evident in the phase data for the isolated airfoil than previous isolated airfoil cases and the other solidity values. In this case, the data are seen to correlate trendwise with the prediction over the front of the vane, then decrease slightly lower than the prediction and remain almost constant for the remainder of the vane. In addition, the phase data for these two configurations correlate quite well with one another over almost the entire vane. Comparing these results to the phase data of Fig. 8 for a $(\hat{u}^+/\hat{v}^+)$ of 0.218 indicates that loading has a dramatic effect on the phase as well as the magnitude data: Both the phase and the magnitude data show the maximum deviations from the analysis in the 25 to 50 percent chord locations. Aft of this point the magnitude and phase increase to the prediction.

The differences apparent in the dynamic pressure difference coefficient phase data for the three different solidity values are a result of the details of the steady static pressure distributions and the spacing between the airfoils. As the airfoil spacing increases for low levels of aerodynamic loading, the correlation of the phase data with the predictions gets increasingly better. This indicates that the influence of adjacent airfoils is much greater than predicted by the zero incidence flat plate analysis.

Thus, both the transverse and chordwise gust components affect the magnitude data, with the chordwise gust having a larger influence on the phase, particularly at the design solidity. In addition, the magnitude of the chordwise gust is not small as compared to either the absolute velocity or the transverse gust.

Potential Flow Interactions

Data in the vane trailing edge region are consistently increased relative to the prediction. Part of this increase is attributable to the chordwise gust that is not modeled by the prediction. However, first-stage magnitude data exhibit larger deviations in the trailing edge region than third-stage data with similar steady lift coefficients. To investigate this phenomenon, unsteady data are acquired on the second and third stages at the design solidity for operating conditions where the steady loading and the forcing function are nearly identical (Fig. 12). Thus the only difference between these two configurations is the presence of the third stage downstream of the second-stage stator row.

The resulting dynamic pressure difference coefficient data and corresponding prediction are presented in Fig. 13. The magnitude data are decreased relative to the prediction over the leading 30 percent of the vane due to the steady loading level, with the deviations in the amplitude attributed to the differences in the steady surface pressure distributions in the leading edge region. Aft of 30 percent chord, the data increase to the level of the prediction, with the second-stage data higher in amplitude than the third-stage data, particularly in the trailing edge region. Since the steady pressure distributions and the forcing function are nearly identical, this deviation of the second-stage data is attributed to a potential interaction effect caused by the downstream third stage. The increase of the third-stage data above the prediction in this region is a result of the chordwise gust since there are no downstream airfoil rows, with the further increase in the second-stage data due to the potential interaction.

The phase data also show different trends in the trailing edge region due to potential interactions. Over the front part of the vane, the data are increased with respect to the prediction, but then decrease in relation to the prediction at 22 percent chord. The data then increase until 50 percent chord, with the data up to this point exhibiting good trendwise correlation. Aft of 50 percent chord the second-stage data are nearly constant with increasing chordwise position, whereas the third-

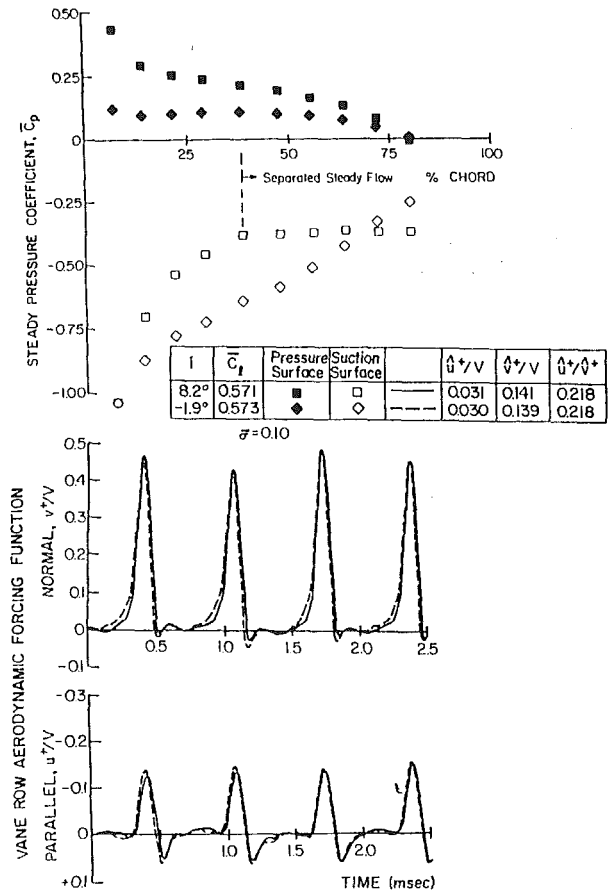

Fig. 14 Steady loading and forcing functions for isolated airfoil separated flow investigation

stage data show another decrease in phase and then increase with increasing chordwise position.

Thus, potential interaction effects influence both the magnitude and phase, with the larger effect being upon the magnitude of the dynamic pressure difference coefficient. Hence, the downstream airfoil row is another aerodynamic excitation source to the upstream blade or vane row and would act on the trailing edge region.

Isolated Airfoil Separation

The effect of separated flow on the stator vane unsteady aerodynamics for a solidity of 0.10, i.e., an isolated airfoil, is now investigated. The separated flow is generated by restaggering the stator vanes such that a mean flow incidence angle of 8.2 deg is established. At this incidence angle, the flow separates from the vane suction surface as indicated by the region of constant static pressure, which originates at 38 percent chord (Fig. 14). The separated flow data are compared with data for a configuration where the steady lift coefficient and both the chordwise and transverse gust componets are nearly identical, but the flow is not separated.

The resulting dynamic pressure difference coefficient data and the attached flow flat plate prediction are shown in Fig. 15. The attached and separated flow data show somewhat different trends in the leading and trailing edge regions. The separated flow magnitude data are nearly constant over the front 14 percent of the vane, whereas the attached flow data and prediction indicate a decrease in amplitude with increasing chordwise position. Aft of 14 percent chord the data show analogous trends, with both separated and attached flow data decreasing with increasing chordwise position and attaining a minimum amplitude value at 20 percent chord, similar to previous isolated airfoil results. The magnitude data for both

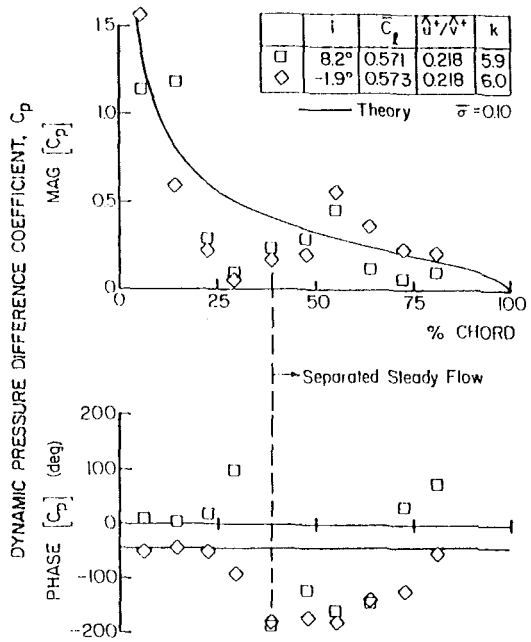

Fig. 15 Steady suction surface separation effect on the complex unsteady pressure coefficient

cases then gradually increase to values that are greater than the prediction at 54 percent chord, with the attached flow data being lower in magnitude up to this point. Both data sets then decrease with further chordwise position, with the separated data decreased in amplitude relative to both the prediction and the attached flow data. This is a result of the increased steady loading in this region of the airfoil due to the separation zone.

The attached and separated flow phase data have different trends near the separation point and in the trailing edge region. Over the front 22 percent of the vane, the data and the prediction show analogous trends, being nearly constant. The separated data are increased relative to the prediction, with the attached flow data exhibiting excellent correlation with the prediction. Aft of 22 percent chord the separated data increase, whereas the attached flow data decrease relative to the prediction. In the separated flow region, both the separated and attached flow data exhibit similar trends. However, at 70 percent chord the separated data indicate a jump to values larger than the prediction and increase with further chordwise position. On the other hand, the attached flow phase data show a gradual increase. Thus, separation affects both the magnitude and phase of the dynamic pressure difference coefficient.

Summary and Conclusions

A series of experiments were performed to investigate the wake-generated gust aerodynamics on each vane row of a three-stage axial flow research compressor at high reduced frequency values, including multistage interactions. In these experiments, the effects, on vane row unsteady aerodynamics of the following were investigated and quantified: (1) steady vane aerodynamic loading; (2) aerodynamic forcing function waveform, including both the chordwise and transverse gust components; (3) solidity; (4) potential interactions; and (5) isolated airfoil steady flow separation. The analysis of these unique vane row unsteady aerodynamic data determined the following.

- The steady aerodynamic loading level, not the incidence angle, is the key parameter to obtain good correlation with flat plate cascade gust models.
- The steady loading level and chordwise loading distribution have a significant effect on vane row unsteady

aerodynamics, having a larger influence on the magnitude than on the phase.

- The aerodynamic forcing function chordwise gust affects both the dynamic pressure coefficient magnitude and phase, whereas the transverse gust primarily affects the magnitude. These effects cannot be predicted with harmonic gust models because these data have been Fourier decomposed, with the predictions thus identical for all forcing function waveforms.
- The chordwise gust is not small compared to either the absolute velocity or the transverse gust. Thus, to provide accurate predictions, unsteady aerodynamic models must consider this gust component.
- For closely spaced stages (the compressor rotor–stator axial spacing herein is 0.432 chord), downstream airfoil rows are potential aerodynamic excitation sources, which affect the unsteady loading in the trailing edge region of the upstream airfoils. Since the trailing edge is thin, it would be highly susceptible to fatigue failure.
- Flow separation of the low solidity vane row affects the unsteady surface pressures upstream of the separation point, with the phase affected in the trailing edge region.

Acknowledgments

Support of this research program by the Air Force Office of Scientific Research, Dr. James Wilson, program manager, is most gratefully acknowledged.

References

Atassi, H. M., 1984, "The Sears Problem for a Lifting Airfoil Revisited—New Results," *Journal of Fluid Mechanics*, Vol. 141, pp. 109–122.

Capece, V. R., Manwaring, S. R., and Fleeter, S., 1986, "Unsteady Blade Row Interactions in a Multi-stage Compressor," *AIAA Journal of Propulsion*, Vol. 2, No. 2, pp. 168–174.

Capece, V. R., and Fleeter, S., 1987, "Unsteady Aerodynamic Interactions in a Multi-stage Compressor," ASME JOURNAL OF TURBOMACHINERY, Vol. 109, No. 3, pp. 420–428.

Carta, F. O., and St. Hilaire, A. O., 1979, "Effect of Interblade Phase Angle and Incidence Angle on Cascade Pitching Stability," ASME Paper No. 79-GT-153.

Carta, F. O., 1982, "An Experimental Investigation of Gapwise Periodicity and Unsteady Aerodynamic Response in an Oscillating Cascade, Part I: Experimental and Theoretical Results," NASA CR 3513.

Chiang, H. D., and Fleeter, S., 1988, "Prediction of Loaded Airfoil Unsteady Aerodynamic Gust Response by a Locally Analytical Method," *International Journal of Mathematical Modeling*, in press.

Englert, G. W., 1982, "Interaction of Upstream Flow Distortions With High Mach Number Cascades," ASME Paper No. 82-GT-137.

Fleeter, S., 1973, "Fluctuating Lift and Moment Coefficients for Cascaded Airfoils in Nonuniform Compressible Flow," *AIAA Journal of Aircraft*, Vol. 10, pp. 93–98.

Fleeter, S., Jay, R. L., and Bennett, W. A., 1978, "Rotor Wake Generated Unsteady Aerodynamic Response of a Compressor Stator," ASME *Journal of Engineering for Power*, Vol. 100, pp. 664–675.

Fleeter, S., Bennett, W. A., and Jay, R. L., 1980, "The Time Variant Aerodynamic Response of a Stator Row Including the Effects of Airfoil Camber," ASME *Journal of Engineering for Power*, Vol. 102, pp. 334–343.

Fleeter, S., Jay, R. L., and Bennett, W. A., 1981, "Wake Induced Time Variant Aerodynamics Including Rotor-Stator Axial Spacing Effects," ASME *Journal of Fluids Engineering*, Vol. 103, No. 1, pp. 59–66.

Gostelow, J. P., 1977, "A New Approach to the Experimental Study of Turbomachinery Flow Phenomena," ASME *Journal of Engineering for Power*, Vol. 99, pp. 97–105.

Hardin, L. W., Carta, F. O., and Verdon, J. M., 1987, "Unsteady Aerodynamic Measurements on a Rotating Compressor Blade Row at Low Mach Number," ASME JOURNAL OF TURBOMACHINERY, Vol. 109, No. 4, pp. 499–507.

Verdon, J. M., and Caspar, J. R., 1981, "Development of an Unsteady Aerodynamic Analysis for Finite Deflection Subsonic Cascades," NASA CR 3455.